Available online at www.sciencedirect.com

ScienceDirect

Procedia CIRP 94 (2020) 414–418

www.elsevier.com/locate/procedia

11th CIRP Conference on Photonic Technologies [LANE 2020] on September 7-10, 2020

Assessment and verification of mean effective diameter of internal channels fabricated by laser powder bed fusion

Lokesh Chandrabalan[a,b,*], Markus Baier[b], Roberto Meloni[a], Luca Ammannato[a], Eugenio Del Puglia[a], Simone Carmignato[b]

[a]*Baker Hughes, Via Felice Matteucci 2, 50127 Florence, Italy*
[b]*University of Padova, Department of Management and Engineering, Stradella S. Nicola 3, 36100 Vicenza, Italy*

* Corresponding author. Tel.: +39-351-053-5522 ; *E-mail address:* Lokesh.Chandrabalan@bakerhughes.com

---

Abstract

Channels with small diameters, used for example in conformal cooling, can nowadays be fabricated by laser powder bed fusion. Measurements of the mean effective diameter and surface topography are important to quantify the flow capabilities through the channel. In this paper, a new method using X-ray computed tomography is developed to obtain the mean effective diameter and mean surface topography height. The developed method is verified by determining the mean effective diameter using incompressible turbulent fluid flow simulations, whereupon the determined mean surface topography height is fed as an input to the simulation. The method is proved to offer a non-destructive and relatively fast approach to measure the mean effective diameter and mean surface topography height in circular channels.

Keywords: Industrial X-ray computed tomography; laser powder bed fusion; mean effective diameter; mean surface topography height; incompressible turbulent fluid flow

---

1. Introduction

The process capabilities of metal additive manufacturing are improving drastically, now allowing the fabrication of intricate structures with reduced deviations and errors [1]. The production of channels with small diameters and different inclinations has always been of significant interest in manufacturing advanced industrial components, such as gas turbine parts. With the aid of laser powder bed fusion (L-PBF) process, the fabrication of internal channels in metallic parts has been made easier and rapid. However, a major challenge lies in the dimensional and quality assessment of the produced part. Furthermore, the surface of additively manufactured channels is subject to high surface irregularities, which could potentially affect the channels' functionality, for example causing pressure drop and heat transfer reduction [1,2]. Therefore, the mean effective diameter affected by the microscale surface irregularities must be carefully analyzed in a non-destructive manner to understand the effects on the functionality of the channel [1].

X-ray computed tomography (CT) offers the advantage of non-destructively assessing the fabricated parts both internally and externally over a wide variety of components [3,4]. There are different approaches to perform dimensional and geometrical analyses, such as the nominal to actual comparison analysis on the CT scanned part using different post-processing

10.1016/j.procir.2020.09.156

software [5]. However, for parts with high surface irregularities and deformations, the alignment between the nominal (CAD model) and the actual (CT) geometry of the scanned part is prone to bias and errors, which can impair the accuracy of the dimensional assessment [5]. Especially, in the case of channels fabricated by laser powder bed fusion process (L-PBF) deviating from the build platform, poor surface quality can be witnessed predominantly due to several causes such as stair-case effect or sag and dross formations.

To overcome these hurdles, a new method is proposed in this paper to assess the mean diameter and internal surface topography of cylindrical channels fabricated by L-PBF with respect to the functionality of the part. Using algorithms for ‘wall thickness analysis’ in VGStudio MAX 3.3 (Volume Graphics GmbH, Germany) which are based on the voxel grey values of the scanned volume [6], it is possible to analyse the part geometrical deviations without the necessity of an alignment with the nominal object. In particular, in this work wall thickness analysis is performed on the CT reconstructed volume inside a specific region of interest, including only the internal channel to avoid contributions from the external deviations. The method is applied once operating in background (i.e. the volume inside the channel) and once in material mode. The resulting thickness histograms are used to obtain the mean diameter (background mode) and microscale surface features (material mode).

In fluid mechanics, the microscale surface features in the channel are evaluated through functional-related parameters, particularly the so called ‘sand grain roughness’ (k_s) or ‘mean roughness height’ (ε), which is defined as the mean height of tightly packed protruding sand grain like features that are uniformly distributed inside the channel [7]. Further work is needed to correlate the functional-related parameters with standard surface texture parameters. Since metal additive manufacturing technologies have been in use over a short period of time, the research studies on influence of k_s over the functionality in additively manufactured parts are limited [8,11]. Increasing dimensions of microscale surface features in the channel (and corresponding k_s values) lead to increase in friction during fluid flows and affect the mass flow rate due to the resulting pressure drop [2]. As part of this work, the obtained values from wall thickness analysis were compared to flow simulations using ANSYS Fluent 19.2 (ANSYS, Inc., United States of America) to evaluate the corresponding pressure drop throughout the length of the channel and thereby the resulting hydraulic diameter (d_h) were calculated.

The specimen investigated in this study is a cylinder, which is a part of the benchmark artefact proposed in [9], with a nominal internal hole diameter of 1 mm and a wall thickness of 0.8 mm with an overall cylinder length of 19.2 mm. The material used for fabrication was INCONEL 718, which is an austenitic nickel-chromium-based superalloy, commonly used for high temperature applications in gas turbines. The specimen was fabricated vertically with an orientation perpendicular to the build platform. Upon fabrication, the specimen was cut from the build platform by electrical discharge machining (EDM).

Nomenclature

CT	X-ray computed tomography
L-PBF	Laser Powder Bed Fusion
ROI	region of interest
msth	mean surface topography height
k_s	sand grain roughness
ε	mean roughness height
d_h	hydraulic diameter
ΔP	pressure drop
$\dot{m}$	mass flow rate
d_{mean}	mean diameter

2. Methodology

2.1. X-ray Computed Tomography measurements

The component was scanned using a metrological CT system (Nikon MCT 225, Nikon Metrology X-Tek, UK). To be able to resolve the microscale surface features inside the channel, the part was positioned as close as possible to the X-ray source to achieve the highest resolution, resulting in a voxel size of 4 µm. Table 1 represents the optimised scan parameters that were applied to scan the part. Due to the density of the material, a filter of 0.5 mm thickness made of tin was used to reduce beam hardening artefacts. The specimen was CT scanned at its centre, for a total length of the reconstructed channel of around 7 mm. Subsequently, the acquired images were reconstructed with the reconstruction software provided by the CT system manufacturer, without any additional mathematical filtering or artefact reduction. Upon reconstruction, the volume was imported in VGStudio MAX 3.3 for further analysis.

Table 1. Optimized scan parameters used for CT measurements

Parameter	Value
Power	6.8 W
Voltage	170 kV
Exposure time	2 seconds
Number of projections	2000

After surface determination, a region of interest (ROI) comprising only the internal channel was created to perform the wall thickness analysis, in two different modes (background and material). Figure 1 shows the cross-section of the analyzed channel. The section marked in red is the ROI comprising the internal channel. As denoted in the legend of the figure, the direction of the blue and yellow arrows represents the operational direction of the background and material modes. The background mode operates on the internal volume of the channels (i.e. non-material voxels) using the determined surface as the starting point to find the opposite surface under a certain opening angle [10]. On the other hand, the material mode functions in the same manner with the difference that it determines the thickness distribution of the material voxel contained in the ROI. In both the cases, the Ray method was chosen with a search angle of 15° [10]. The resulting wall thickness histograms were exported and further processed with the aid of an in-house developed MATLAB script to obtain the mean diameter and the mean surface topography height *(msth).*

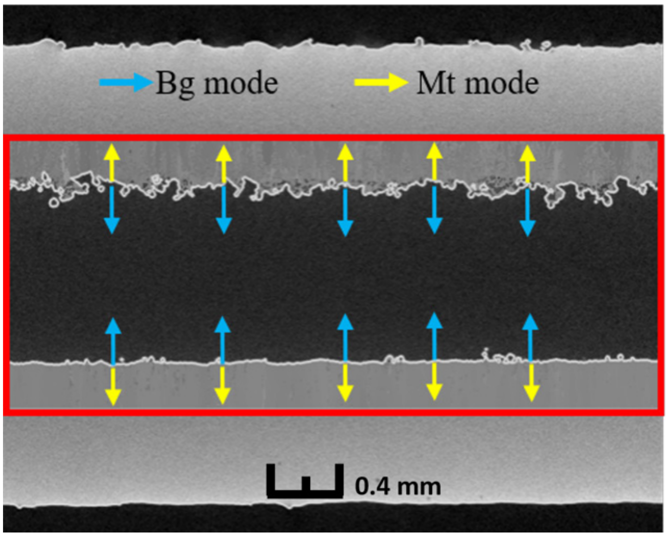

Fig. 1. Cross-section of the analysed channel with the ROI denoted in red. The blue and yellow arrows represent the analysis direction for background and material mode of the wall thickness analysis.

2.2. Application of Computational Fluid Mechanics

Incompressible Reynolds-averaged Navier-Stokes (RANS) turbulent fluid flow simulations were performed with k-ε turbulence model at four different mass flow rates $(\dot{m})$ using ANSYS Fluent. The nominal diameter is used as the channel diameter in the Computational Fluid Mechanics model and the aforementioned *msth* is used as the k_s inside the channel, which is a necessary input to determine the associated pressure drop (ΔP) and the exit fluid flow velocity over a certain channel length [11]. To achieve comparability, the channel length in the CFD model was the same as analyzed by CT. Subsequently, the general mass flow rate $(\dot{m})$ equation was used to calculate the corresponding d_h. To perform high fidelity simulations, polyhedral mesh was used, thereby increasing the accuracy. Furthermore, to achieve fully developed turbulent flow at the inlet of the channel, the length of the channel was extruded 10 times more before the actual inlet. In addition, the theoretical pressure-drop and the friction factor for the mean diameter and *msth* were calculated using the Colebrook-White and Darcy–Weisbach equations, as a theoretical reference case [12].

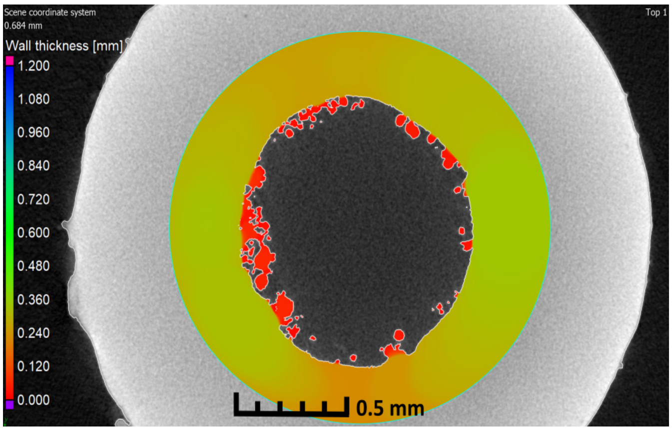

Fig. 2. Cross-sectional view of the wall thickness analysis performed in material mode on the channel, revealing the microscale surface features in red.

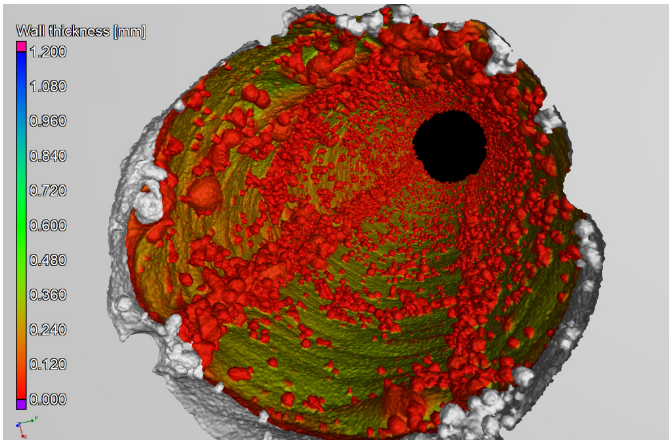

Fig. 3. 3D rendering view of the wall thickness analysis performed in material mode on the 1 mm channel over a total length of 6.8 mm, revealing the microscale surface features in red.

3. Results and discussion

The results discussed in this paper do not reflect the actual additive manufacturing capabilities of Baker Hughes. Figure 2 shows a cross-sectional view of the analyzed channel perpendicular to channel direction, whereas Figure 3 displays a 3D rendering of the wall thickness analysis performed in material mode inside the ROI. The microscale surface features show sizes up to 120 µm (shown in red in Figures 2 and 3). Analyzing the 3D rendering, there is a trend in the distribution of the surface features leading to an increased number of particles on one side of the channel, which is caused by the interaction between the previously printed layer and the re-coater, while spreading a new powder layer. Furthermore, from Figure 3, it is evident that the microscale surface features have an anisotropic distribution.

The cropped wall thickness histograms and the corresponding Gaussian fits of the CT analysis are shown in Figure 4 and 5. The fits are performed in a selected region around the main peak avoiding the tails where it includes features that do not correspond either to the microscale surface features or to the channel diameter, but are rather intermediate distances caused by the methodology involved in the wall thickness analysis. Figure 4 shows the obtained *msth* with the centre of the fitted Gaussian at 25 µm. In this case, the fitting was performed between 0 to 50 µm. On the other hand, Figure 5 displays the histogram data and the Gaussian fit for the mean internal channel diameter, resulting in a mean diameter of 0.93 mm, which is a reduction of 70 µm with respect to the design value. In this case, the range for the Gaussian was chosen again around the centre of the main peak considering the histogram data between 880 µm and 1100 µm. As mentioned above, the determined *msth* is used in the flow simulations to verify the mean channel diameter obtained by CT.

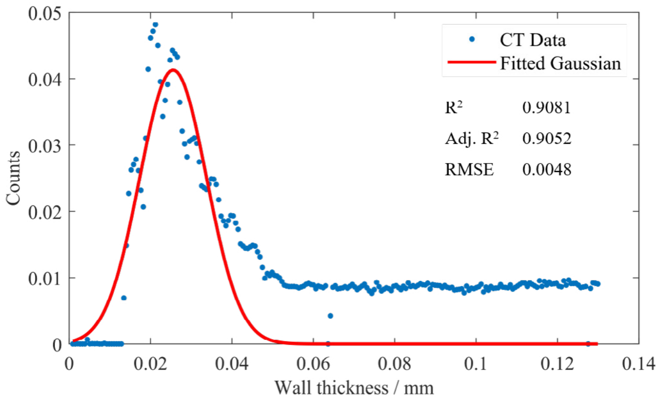

Fig. 4. Wall thickness histogram with fitted Gaussian for *msth*.

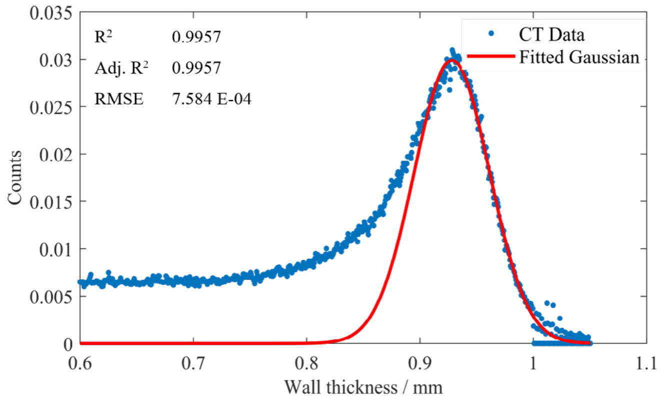

Fig. 5. Wall thickness histogram with fitted Gaussian for mean internal channel diameter.

The developed CFD model and the axial velocity contour plot of an incompressible turbulent fluid flow simulation are shown in Figure 4 and Figure 5 respectively. The *msth* of 25 µm from the wall thickness analysis in the material mode was given as an input for ε in ANSYS Fluent, only in the domain consisting the actual length of the channel excluding the additional extruded length before the inlet [11].

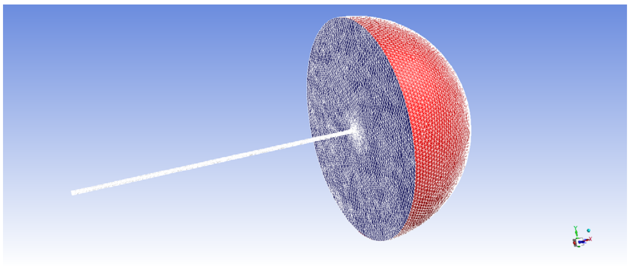

Fig. 6. Developed CFD model for incompressible turbulent fluid flow simulations.

The results of the incompressible turbulent fluid flow simulations at different $\dot{m}$ and the corresponding theoretical values are summarized in Table 2. The theoretical and the calculated pressure drop *(ΔP)* values from the CFD simulations are in line, with an error less than 1%. This indicates that the obtained *msth* from CT is equivalent to k_s or ε in circular pipe flows. Since the channel has a cylindrical geometry, the mean diameter from the wall thickness method is equivalent to the calculated hydraulic diameter from the incompressible turbulent fluid flow simulations. The calculated d_h, at all mass flow rates, has a deviation of less than 1.5% from the mean internal channel diameter obtained from CT. This additionally confirms the hypothesis of *msth* corresponding to ε or k_s and verifies that the mean channel diameter is equivalent to the hydraulic diameter.

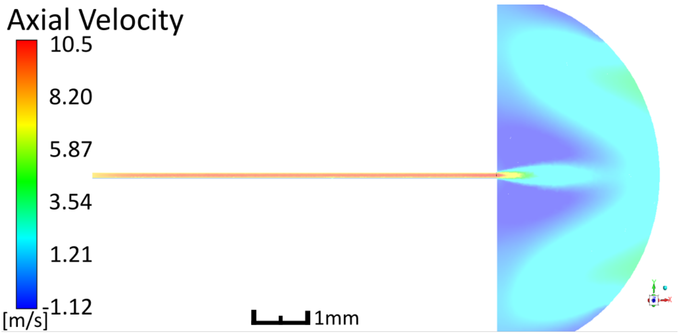

Fig. 7. Exemplary axial velocity contour plot.

Table 2. Comparison of theoretical and simulated results, d_h based on CFD simulations

$\dot{m}$ (kg/s)	ΔP (Pa) (Theoretical)	ΔP (Pa) (Simulation)	d_h (mm)	$\Delta P_{the.}$ vs $\Delta P_{sim.}$ (% Error)	$d_{mean.}$ vs d_h (% Error)
0.004	7522	7455	0.916	0.89	1.26
0.0055	13925	13963	0.915	0.27	1.40
0.007	22272	22305	0.914	0.14	1.47
0.0085	32565	32376	0.914	0.58	1.47

4. Conclusions

The study focused on developing a new approach using CT to determine the mean effective diameter and internal microscale surface features of cylindrical channels fabricated by L-PBF, taking strongly into consideration the flow functionality of the component. The mean channel diameter obtained from CT was verified by comparison with the calculated hydraulic diameter from CFD simulations, showing deviations less than 1.5%.

The obtained pressure-drops for different mass flow rates from the CFD simulations were compared to the reference case. The comparison studies showed error less than 1%, confirming the hypothesis that the mean surface topography height corresponds to k_s or ε in circular channel.

The results presented in this work are the first proof of concept of the proposed method. Future work will include analyzing inclined channels with high surface irregularities due to stair-case effects and dross formations and thereby verify and correlate the concept of k_s. Furthermore, the methodology will be validated with experimental flow tests on different internal channel geometries, with respect to actual applications.

Acknowledgements

This work was made within PAM^2, ‘Precision Additive Metal Manufacturing’, a research project funded by The EU Framework Programme for Research and Innovation - Horizon 2020 - Grant Agreement No 721383.

References

[1] Stimpson CK, Snyder JC, Thole KA, Mongillo D. Scaling roughness effects on pressure loss and heat transfer of additively manufactured channels. J. Turbomachinery 2017; 139, 021003.

[2] Klingaa, CG, Bjeree MK, Baier S, De Chiffre L, Mohanty S, Hattel JH. Roughness Investigation of SLM Manufactured Conformal Cooling Channels Using X-Ray Computed Tomography. 9th Conference on Industrial Computed Tomography 2019, Padova, Italy.

[3] Kraemer A, Lanza G. Assessment of the measurement proceudre for dimenional metrology with X-ray computed tomography. 14th CIRP Conference on Computer Aided Tolerancing (CAT) 2016; Procedia CIRP 43. p.362 – 367.

[4] Aloisi V, Carmignato S. Influence of surface roughness on X-Ray computed Intomography dimensional measurements of additive manufactured parts. Case Studies in Nondestructive Testing and Evaluation 2016; 6. p.104-110.

[5] Kruth JP, Bartscher M, Carmignato S, Schmitt R, De Chiffre L, Weckenmenn A. Computed Tomography for Dimensional Metrology. CIRP Annals - Manufacturing Technology 2011; 60(2). p.821-842.

[6] du Plessis A, Rossouvw P. X-ray computed tomography of a titanium aerospace investment casting. Case Studies in Nondestructive Testing and Evaluation 2015; 3. p. 21-26

[7] Arshad FF, Rieke HH. Surface-Roughness Design Values for Modern Pipes. SPE Drilling & Completion 2006.

[8] Stimpson CK, Snyder JC, Thole KA, Mongillo D. Roughness Effects on Flow and Heat Transfer for Additively Manufactured Channels. J.Turbomachinery 2016; 138, 051008.

[9] Chandrabalan L, Matoni E, Malarco M, Del Puglia E, Ammannato L, Carmignato S. Investigation on precision of laser powder bed fusion process using statistical process control. Joint Special Interest Group meeting between euspen and ASPE. Advancing precision in Additive Manufacturing 2019. Nantes, France.

[10] Sbettega E, Zanini F, Benedetti M, Savio E, Carmignato S. X-ray computed tomography dimensional measurements of powder fusion cellular structures. euspen's 18th International Conference & Exhibition 2018. Venice, Italy.

[11] Kilpatrick E, Sung K. Roughness effects on flow and heat transfer in a ribbed duct considering additive manufacturing. Global Power and Propulsion Society Forum 2018. Zurich, Switzerland.

[12] Nikuradse J. Laws of Flow in Rough Pipes. 1933; NACA Technical Memorandum 1292.